Solid Freeform Fabrication 2024: Proceedings of the 35th Annual International
Solid Freeform Fabrication Symposium – An Additive Manufacturing Conference
Reviewed Paper

Investigation of the Homogenized Anisotropy for the Triply Periodic Minimal Surface Lattice under Varying Applied Stress Orientation

Chongyi Wei, Douglas E Smith*
Department of Mechanical Engineering, Baylor University, Waco, TX 76706
* Corresponding author: douglas_e_smith@baylor.edu

Abstract

The advance of additive manufacturing makes it possible to design spatially varying lattice structures with complex geometric configurations. The homogenized elastic properties of these periodic lattice structures are known to deviate significantly from isotropic behavior where orthotropic material symmetry is often assumed. This paper addresses the need for a robust homogenization method for evaluating anisotropy of periodic lattice structures including an understanding of how the elastic properties transform under rotation. Here, periodic boundary conditions are applied on two-material representative volume element (RVE) finite element models to evaluate the complete homogenized stiffness tensor. A constrained multi-output regression approach is proposed to evaluate the elasticity tensor components under any assumed material symmetry model. This approach is applied to various lattice structures including scaffold and surface-based Triply Periodic Minimal Surface (TPMS). Our approach is used to assess the accuracy of rotation for assumed anisotropic and orthotropic homogenized material models over a range of lattice structures.

1 Introduction

Advances in Additive Manufacturing (AM) make it possible to fabricate more complex structures than what was previously possible with traditional manufacturing methods, therefore, AM has become the primary choice to produce cellular lattice structures. The cellular lattice is of research interest that focuses on improving the mechanical behavior of complex microstructures inspired by nature, such as those found in bones, wood, and honeycomb structures. Cellular structures have multiple advantages such as lightweight and improved designability resulting in a wide range of applications. Among them, TPMS lattices are of particular interest in the field of cellular design due to their smooth surfaces, high interconnectivity porous architectures, and mathematically controllable geometry. TPMS lattice structures consist of smooth surfaces with zero mean curvature which eliminates local stress concentrations, unlike strut-based lattice structures which do not provide this benefit to the design community [1].

The variable ligament size and orientation of TPMS structures with symmetry in all three dimensions lead to anisotropy which typically requires finite element analysis (FEA) to determine the homogenized elasticity in different directions. It has been shown that TPMS structures have a relatively high level of directional dependency on homogenized elastic tensors and typically present anisotropic behavior leading to directions of high and low stiffness and strength, especially when the relative density is low [2]. As a result, numerical homogenization theory and FEA methods are often applied to determine the relationship between mathematical parameters that describe the TPMS geometry and the structure's effective elastic modulus and other related anisotropic properties [3]. The homogenization method is used to bridge between macrostructure

and microstructure representation, in which the goal is often to obtain effective values for elastic tensor components. The homogenized elastic modulus of TPMS unit cells has been predicted by FEA using periodic boundary conditions and a fast Fourier transform-based homogenization method [4,5], and has been shown to vary linearly with relative density. Additionally, Khaleghi et al. [6] showed that hybrid lattice structures have a more isotropic-oriented effective elastic modulus compared to their parent lattice structures, and an appropriate selection of the combination ratio of the parent structures can lead to minimal anisotropy.

Anisotropy can be an undesirable property when the lattice structure is exposed to unknown directional loads, especially in energy-absorbing applications. However, when anisotropy plays an important role in influencing the mechanical properties of a lattice structure, it is necessary to consider anisotropic properties while modeling the spatially varying lattice structures with variant orientation in the design layout [7]. The 3D triply periodic minimal surface lattice plates (RotTPMS) were designed to an optimal lattice orientation on the basis of the anisotropy's porosity dependence [8]. Since the TPMS mechanical properties strongly depend on the relative density [2], the relative density may be adjusted to keep consistency by changing the location of the implicit surface function for a TPMS structure. Additionally, anisotropy may change as well as the change of relative density and the topological distribution due to the rotation of lattice structures.

Anisotropy for TPMS lattice structures is usually measured by the Zener index based on only three terms from the homogenized elasticity tensor [9]. For the Zener index to be applied, it must be assumed that the orthotropic material model is applicable when obtaining the homogenized elastic tenors for lattice structures. It follows that the rotational behavior for the homogenized elasticity tensors is often obtained by applying the rotational matrix under the orthotropic material assumption. However, the rotation of a lattice structures' homogenized elasticity tensor may not coincide with the actual response under a rotated loading condition. Therefore, the TPMS with spatially varying orientation [7] may experience loading from a wide range of angles, which inspires us to evaluate the anisotropy under variant orientations such as the application of rotation matrix on an element-by-element basis of stress-strain. Here, this study presents a novel material fitting model based on the homogenized elastic matrix for the TPMS lattice structures to evaluate the difference between orthotropic and anisotropic fitting models. The element-by-element and homogenized rotational bases are proposed to investigate the anisotropy for various lattice structures. The regression coefficients from material fitting model may be viewed as an indicator to measure the anisotropy under rotation.

2 Methodology

The following section will introduce the construction of finite element model for the lattice structures, the homogenization procedures, and the constrained multi-output regression approach, and the rotational basis for homogenized elastic tensors.

2.1 The modeling of TPMS lattice

The TPMS-based lattice structures can be classified into two groups such as surface and scaffold-based ones, which can be modeled by offsetting the implicit surface defined by the generalized level set function [10] as Eq. (1) and the enclosure of implicit surface with surrounding cubic RVE,

respectively. The strut-based lattice is modeled by the selective deletion of elements in the cubic RVE following the Laplacian mesh smooth or the surface smoothing by subdivision [11].

$$F(\boldsymbol{r}) = \sum_{m=1}^{M} \boldsymbol{\mu}_m \cos\left(2\pi(\boldsymbol{p}_m \cdot \boldsymbol{r})\right) + t = 0 \tag{1}$$

where $\boldsymbol{\mu}_m$ is periodic amplitude, $\boldsymbol{p}_m$ is the reciprocal matrix, $\boldsymbol{r}$ is the position vector, and t adjusts the relative density of the TPMS lattice. The end-cap geometry is computed on the computational grid for the volume data $F(\boldsymbol{r})$ with difference enclosure options to model lattice and void space for TPMS lattice structures, the scaffold-based TPMS is shown as Fig. 1. The tetrahedron elements are filled inside the close surface patch forming the implicit surface for the TPMS lattice. A special Boolean operation algorithm based on the MATLAB polygon operation [12] is developed for the strut-based lattice to acquire the exterior (or void) mesh where the material properties are set as trivial values. The two materials phases model for the Cubic strut-based lattice shown in Fig. 2 considers not only the lattice filled with tetrahedron mesh but the void space inclusion between the lattice surface and cubic RVE faces, the material property for the void space is assigned as a trivial value.

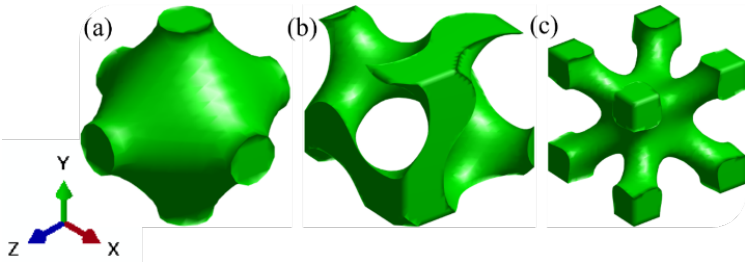

Figure 1: Scaffold-based TPMS unit cell: (a) Primitive; (b) Gyroid; (c) IWP

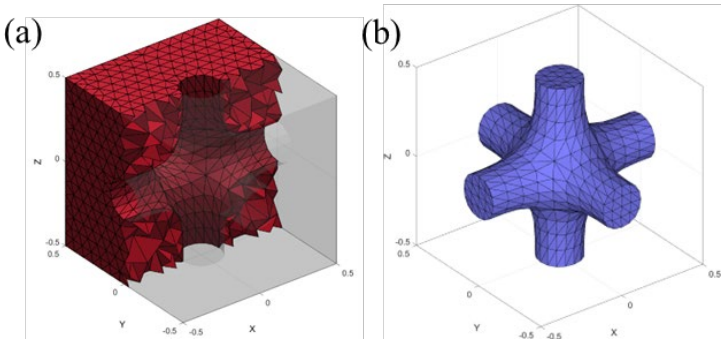

Figure 2 The two-phase mesh for Cubic struct-based lattice unit cell: (a) the mesh for void space; (b) the mesh for Cubic lattice unit cell

2.2 Homogenized model of lattice structure

The homogenized elastic tensors are of importance for the future application of lattice structures as the basic mechanical properties, it is known to deviate significantly from the isotropic behavior where orthotropic material symmetry is often assumed. Obtaining the homogenized elastic properties of the lattice structure is crucial, especially for TPMS structures having a wide range of relative volume fractions. The voxel-based FEA with asymptotic homogenization [13] which is

wide-adopted in the literature [14] may contribute to the inaccuracy of homogenization results due to the hexahedral stair-step mesh, while the implicit TPMS equation (cf. Eq. (1)) leads to the symmetric triangular surface patch (cf. Fig. 1).

2.2.1 The homogenization under periodic boundary conditions

A numerical homogenization method is employed in this work to calculate homogenized elastic properties (i.e., components of the elasticity tensor) for the lattice structures defined above. To predict the homogenized properties by the finite element method, periodic boundary conditions are defined on a representative volume element (RVE) of a single lattice. We adopted a novel approach based on polynomial edge interpolation that avoids the need to match mesh conditions on opposing RVE boundaries similar to that presented in [15]. To implement this approach, a nodal mapping is created that connects nodes on opposing sides of the RVE to define the periodic boundary conditions written as

$$\boldsymbol{u}_i^+ - \boldsymbol{u}_i^- = \bar{\boldsymbol{\varepsilon}}(\boldsymbol{x}_i^+ - \boldsymbol{x}_i^-), \qquad i = 1, \cdots p \tag{2}$$

where $\boldsymbol{u}_i^+$ and $\boldsymbol{u}_i^-$ are the displacements on opposing sides of the RVE, $\bar{\boldsymbol{\varepsilon}}$ defines the imposed macroscopic strain and $(\boldsymbol{x}_i^+ - \boldsymbol{x}_i^-)$ is the distance between opposing nodes on RVE faces. All nodes on the opposite faces, edges and corners are tied by constraints equations on the cubic RVE. Six independent loading conditions with unit strain are applied to the RVE to obtain homogenized elasticity matrix components [16]. These six loading conditions include three uniaxial extensions and six pure shear conditions which are defined such that only the constraint equations on the surface are applied on the unit cell RVE (cf. Fig. 2(a)) where the unit lattice structure and void are included. Once the finite element analysis is performed, the volume-average stress $\bar{\sigma}_{ij}$ and strain $\bar{\varepsilon}_{ij}$ tensor components may respectively be calculated via the integrals as

$$\bar{\sigma}_{ij} = \frac{1}{V}\int_V \sigma_{ij}\, dV \qquad \text{and} \qquad \bar{\varepsilon}_{ij} = \frac{1}{V}\int_V \varepsilon_{ij}\, dV \tag{3}$$

In the above, σ_{ij} and ε_{ij} are the element stress and strain tensor components, respectively, and V is the volume of the RVE [17].

2.2.2 The material regression model

The three-dimensional homogenized 6×6 elasticity matrix $\bar{\ }$ is computed in a constrained least-squared sense to best-fit average RVE computed stresses assembled in the vector $\bar{\boldsymbol{\sigma}}$ and applied strains in the vector $\bar{\ }$ (cf. Eq. (3)) from the finite element analyses as

$$\bar{\boldsymbol{\sigma}} = \bar{\boldsymbol{C}}\bar{\boldsymbol{\varepsilon}} \tag{4}$$

where the components of the matrix $\bar{\boldsymbol{C}}$ are $\bar{C}_{JK}$, J = 1, …, 6, and K = 1, …, 6. A multi-output regression is defined to compute components in $\bar{\boldsymbol{C}}$ from FEA generated volume-averaged stress-strain pairs $(\bar{\boldsymbol{\varepsilon}}^I, \bar{\boldsymbol{\sigma}}^I)$, I = 1, …, N, where we use N = 6 FEA simulations. A linear system of equations written in terms of the unknown J-th row elasticity tensor components that compose $\bar{\boldsymbol{C}}_J$ as [19]

$$\boldsymbol{Z}^T\boldsymbol{Z}\bar{\boldsymbol{C}}_J^{\boldsymbol{T}} = \boldsymbol{Z}^T\bar{\boldsymbol{\sigma}}_J, \quad J = 1, \ldots, P \tag{5}$$

where

$$\boldsymbol{Z} = [(\bar{\boldsymbol{\varepsilon}}^1)^T \quad (\bar{\boldsymbol{\varepsilon}}^2)^T \quad (\bar{\boldsymbol{\varepsilon}}^3)^T \quad \cdots \quad (\bar{\boldsymbol{\varepsilon}}^N)^T]^T \text{ and } \bar{\boldsymbol{\sigma}}_J = \left[\bar{\sigma}_J^1 \quad \bar{\sigma}_J^2 \quad \bar{\sigma}_J^3 \quad \cdots \quad \bar{\sigma}_J^N\right]^T \tag{6}$$

In the above equations, $(\bar{\boldsymbol{\varepsilon}}^I)^T$, $I = 1, \ldots, N$, are the average strains for I_{th} out of N finite element computed strains. Similarly, $\bar{\sigma}_J^I$, $I = 1, \ldots, N$, is the J-th stress component for the I_{th} out of N finite element computed stresses. To impose constraints on the least squares fitting process, we first rewrite Eq. (5) to include all 6 stress components as

$$\boldsymbol{A}\overline{\boldsymbol{C}} = \boldsymbol{R} \tag{7}$$

which represents 36 equations in the 36 unknown coefficients of the averaged elasticity matrix $\overline{\boldsymbol{C}}$. It follows that the symmetry of $\overline{\boldsymbol{C}}$ and any additional assumed material symmetries may be imposed as constraints on the least square fitting process described above [20] through $\boldsymbol{X}\overline{\boldsymbol{C}} = \boldsymbol{Q}$, where $\boldsymbol{X}$ is a matrix containing relationships that are imposed components of $\overline{\boldsymbol{C}}$. The Lagrange Multiplier method is used to impose the constraints in Eq. (8) onto the system of equations in Eq. (7) which is implemented through

$$\begin{bmatrix} \boldsymbol{A} & \boldsymbol{X}^T \\ \boldsymbol{X} & \boldsymbol{0} \end{bmatrix} \begin{Bmatrix} \overline{\boldsymbol{C}} \\ \boldsymbol{\lambda} \end{Bmatrix} = \begin{Bmatrix} \boldsymbol{R} \\ \boldsymbol{Q} \end{Bmatrix} \tag{8}$$

where $\boldsymbol{\lambda}$ is the Lagrange Multiplier. The size of $\boldsymbol{X}$ and the Lagrange multiplier $\boldsymbol{\lambda}$ depend on the number of constraints imposed on $\overline{\boldsymbol{C}}$. For example, matrix symmetry is imposed on $\overline{\boldsymbol{C}}$ with 15 constraint equations written as

$$\bar{C}_{ij} - \bar{C}_{ji} = 0, \qquad i, j \in 1,2,3,4,5,6, \;\; i \neq j, \qquad i < j \tag{9}$$

Similarly, material symmetries including orthotropic, transversely isotropic, or isotropic may be imposed on $\overline{\boldsymbol{C}}$ by respectively imposing 12, 16 or 19 constraint equations in addition to the 15 matrix symmetry equations in Eq. (9). Once the elasticity tensor components in $\overline{\boldsymbol{C}}$ are computed, regression coefficients are calculated to determine the quality of the least squares solution. The regression coefficient R_J^2 for the J-th stress component is given by

$$R_J^2 = (S_t^J - S_r^J)/S_t^J \tag{10}$$

where the sum of the squared error with respect to the material model fit S_r^J and the sum of the squared error with respect to the mean stress S_t^J are given for the J-th stress component, respectively, as

$$S_r^J = \sum_{I=1}^{N} \left(\bar{\sigma}_J^I - \overline{\boldsymbol{C}}_J \bar{\boldsymbol{\varepsilon}}^I\right)^2 \quad \text{and} \quad S_t^J = \sum_{I=1}^{N} \left(\bar{\sigma}_J^I - \bar{\sigma}_J^{mean}\right)^2 \tag{11}$$

where the J-th mean stress $\bar{\sigma}_J^{mean}$ is defined as the averaged value of $\bar{\sigma}_J$.

2.2.3 The homogenized stress and strain rotation bases

T he two-phase 3D finite element mesh is proposed to implement the homogenization method, which is essential to obtain the same averaged strain with applied unit strain that defines the periodic boundary conditions. In order to investigate the rotational behavior of homogenized

elastic properties for lattice structures under various orientations, the calculated stress-strain data can be treated with two approaches. First, the rotation matrices are applied to the homogenized elastic tensors from the homogenized material model where the fitting procedures are performed based on stresses in the model coordinate system. Alternatively, the rotation matrices are applied to stress-strain data on the element-by-element basis to supply the material fitting model and acquire the homogenized elastic tenors (cf. Eq. (3)). To apply the rotations to the material matrix (first approach), the 6×6 transformation method from [21, 22] is adopted. The rotated material constitutive matrix $\overline{\boldsymbol{C}}'$ is computed as $\overline{\boldsymbol{C}}' = \boldsymbol{T}^{-1}\overline{\boldsymbol{C}}\boldsymbol{T}$, where $\overline{\boldsymbol{C}}$ is the homogenized elasticity matrix from the multi-output material regression model, $\boldsymbol{T}$ is the transformation matrix that can be applied on the Voight 6×6 notation tensor. The rotation tensor applied on the elemental stress-strain tensors (alternate approach) are given as [23], and the volume-average stress and strain tensor components are calculated according to Eq. (3) to obtain the symmetric material model by Eq. (8). The rotational operation for stress and strain tensors [23] are given as

$$\boldsymbol{\varepsilon}' = \boldsymbol{R}^T\boldsymbol{\varepsilon}\boldsymbol{R} \tag{12}$$

$$\boldsymbol{\sigma}' = \boldsymbol{R}^T\boldsymbol{\sigma}\boldsymbol{R} \tag{13}$$

where the rotation matrix $\boldsymbol{R}$ is given as

$$\boldsymbol{R} = \begin{bmatrix} \cos\theta & \sin\theta & 0 \\ -\sin\theta & \cos\theta & 0 \\ 0 & 0 & 1 \end{bmatrix} \tag{14}$$

for a rotation about the Z-direction.

To keep consistent, the same material model (such as orthotropic or anisotropic model) is maintained for the above two material rotation approaches described above. The regression coefficient is calculated after the averaged stress-strain is recovered from the elemental stress-strain tensor rotation. The two rotational bases aim to rotate the homogenized elastic tensor based on global and local levels, respectively. The difference between two bases on the rotational plane which is evaluated by the root mean square error (RMSE)

$$\text{RMSE} = \sqrt{\sum_{i=1}^{N} \left(E_1^i - \hat{E}_1^i\right)^2 / N} \tag{15}$$

where i is a index on the rotational grid (about X from 0-90° firstly, then about Z from 0-90°), N is the total number of points on the same grid, and $E_1^i$and $\hat{E}_1^i$ are the normalized Young's modulus from the two rotational approaches. The RMSE provides insight into two rotation method with various fitting material models for lattice structures. The material model regression coefficients tend to present the fitting performance with the symmetric material model.

3 Results and discussion

Relationships between relative density and homogenized elasticity tensor component values for Primitive scaffold lattice with orthotropic and isotropic material models appear in Fig. 3. These results show slight differences in the trends of the elasticity tensor components for the material symmetry models considered. The Zener index ($A = 2\bar{C}_{44}/(\bar{C}_{11} - \bar{C}_{12})$) is used to quantify how

far the material is from being isotropic where A is 1 for an isotropic case and increases or decreases with increasing anisotropy which is restricted to the lattice with cubic symmetry. It is shown that the Zener index increases with relative RVE density that indicates the anisotropy decreases with increasing relative density in Fig. 3. The regression coefficient R_J^2 for the fit of assumed material symmetry model versus the relative density is shown in Fig. 4. Results show that the regression correlation coefficient increases with the relative density of RVE where the isotropic model both produce low-quality fitting results. The orthotropic model gives the best fitting performance with the regression coefficients for all elasticity tensor components near 1. It is interesting to note that the isotropic model results appear to do quite well overall for the axial extension terms (i.e., R_1^2, R_2^2, and R_3^2), but do far worse for the shear terms.

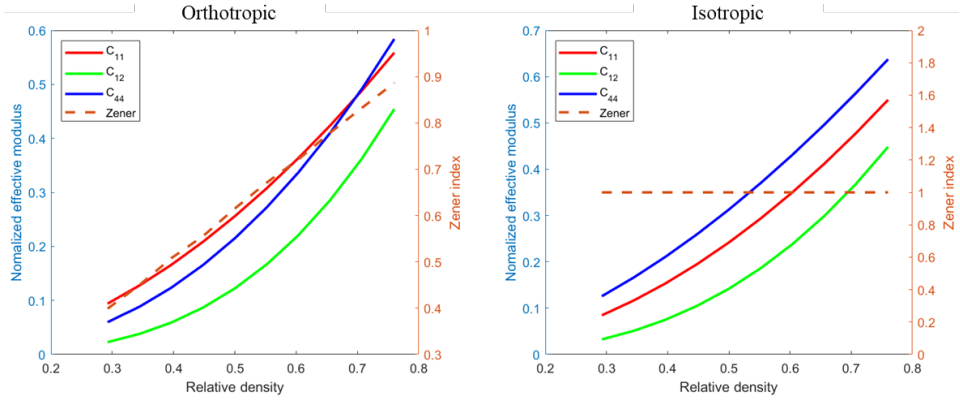

Figure 3. The homogenized elastic tensors versus relative density for Primitive TPMS lattice.

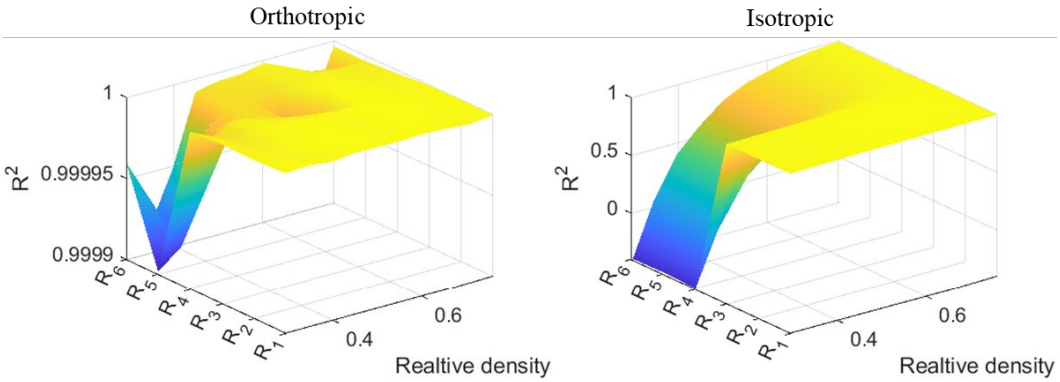

Figure 4. The regression correlation coefficient for four assumed material symmetry models

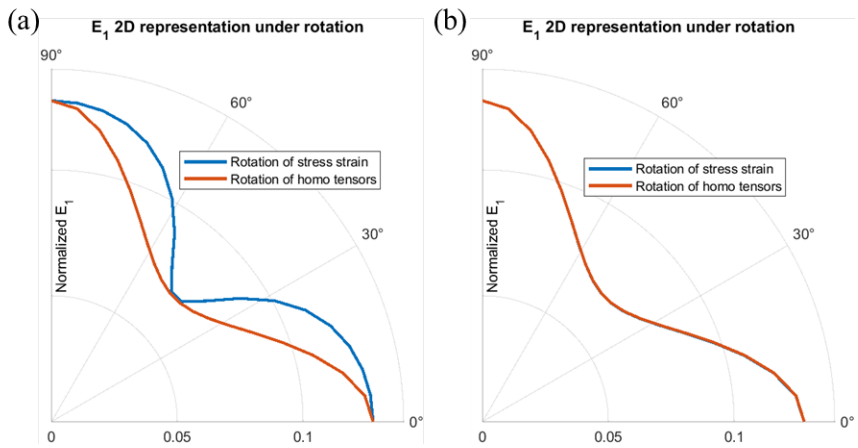

Figure 5: The normalized E_1 of Primitive (with relative density as 0.3) scaffold TPMS lattice under 2D rotation by orthotropic fitting (a), anisotropic fitting (b)

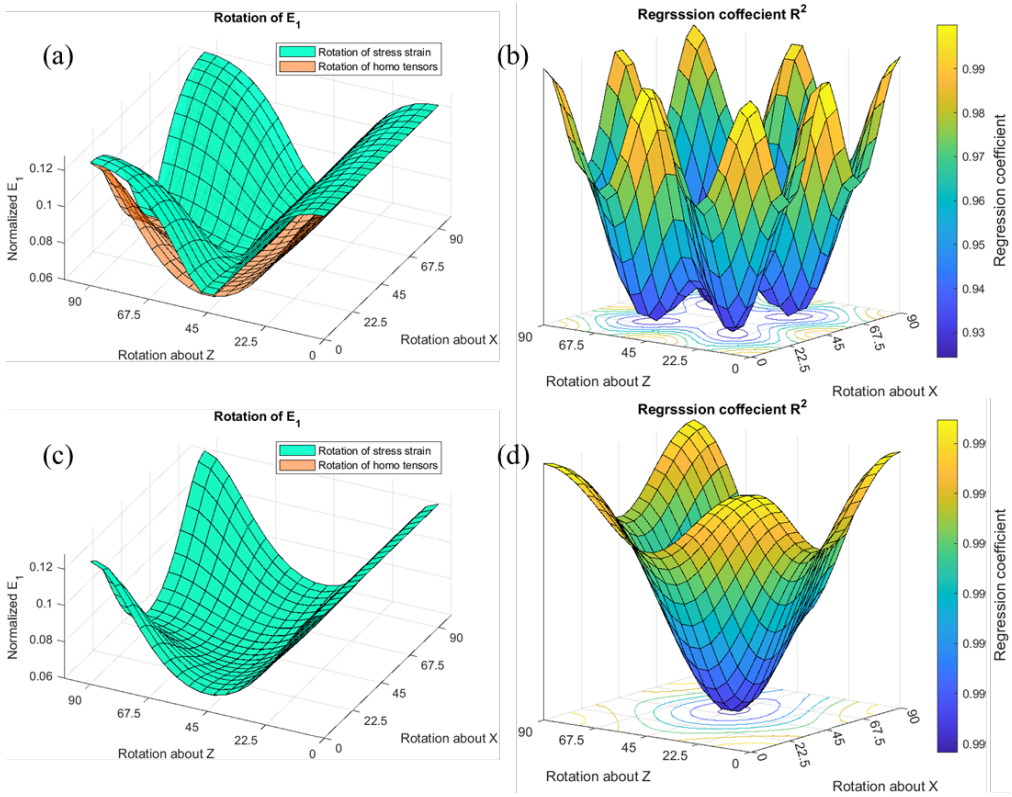

Figure 6: The normalized E_1 of Primitive (with relative density as 0.3) scaffold TPMS lattice under rotation and regression performance by orthotropic fitting (a) and (b); anisotropic fitting (c) and (d)

The evaluation of homogenized elastic tensors by rotation (about Z from 0-90°) based on elemental stress-strain and homogenized elasticity tensor with orthotropic and anisotropic symmetry model fitting show as Fig. 5. Results show that normalized E_1 under 2D rotation with orthotropic fitting only match at 0°, 45°and 90° for two rotational bases, but do match well for all angles when an anisotropic material model is used in the fitting process. The normalized E_1 under 3D rotation

(about X from 0-90° firstly, then about Z from 0-90°) with orthotropic and anisotropic fitting models for the Primitive TPMS lattice are shown as Fig. 6 (a) and (c), the regression coefficients are shown in Fig. 6 (b) and (d). From the 3D surface representation of normalized E_1, it merges with each other for two rotational bases under anisotropic model. Additionally, the anisotropic model provides superior performance by inspecting the regression coefficients, where R^2 is shown rather than R_J^2 (cf. Eqs. (10-11)), such as $S_r = \sum_{J=1}^{N}\sum_{I=1}^{N}\left(\bar{\sigma}_J^I - \overline{\boldsymbol{C}}_J\bar{\boldsymbol{\varepsilon}}^I\right)^2$, $S_t = \sum_{J=1}^{N}\sum_{I=1}^{N}\left(\bar{\sigma}_J^I - \bar{\sigma}_J^{mean}\right)^2$, respectively. The RMSE and regression coefficients together can be treated as indicators that whether the orthotropic fitting model works while rotating in 3D space for a wide range of lattice structures.

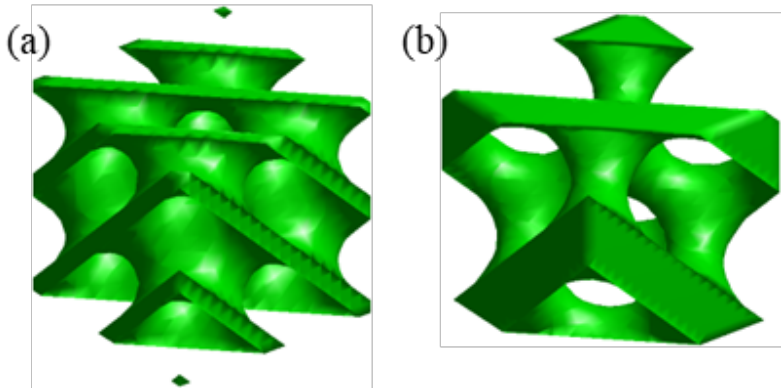

Figure 7: The Diamond TPMS lattice: (a) surface; (b) scaffold

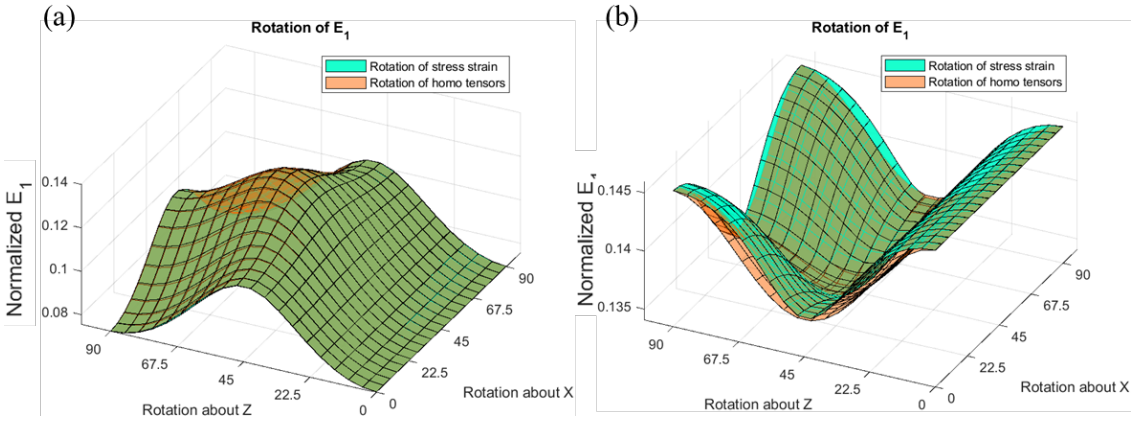

Figure 8: The normalized E1 of Diamond (with relative density as 0.3) for scaffold (a) and surface (b) TPMS lattice under rotation

From the same group of TPMS lattice structures, for instance, the Diamond TPMS with scaffold and surface-based is shown as Fig. 7, it may produce different rotation accuracy under assumed an orthotropic model. The normalized Young's modulus under rotation with assumed orthotropic model is shown in Fig. 8 where there is a difference between the surface-based and scaffold-based structure, which indicates that the scaffold-based Diamondrotates as an orthotropic model on an element-by-element basis. However, the minimal R^2 on the rotational grid for scaffold and surface-based lattice is 0.96 and 0.99 (which is close to the regression performance under

anisotropic model assumption for Primitive scaffold TPMS lattice, as shown in Fig. 6), respectively. The results shown here only consider the normalized uniaxial modulus alone, however, it is expected that similar trends may be found with other homogenized elastic components, such as shear modulus and Poisson's ratio. Therefore, the regression coefficient is shown ot provide a comprehensive indicator on anisotropy for lattice structure under variant orientation.

4 Conclusion

This paper proposes a novel symmetric material model regression approach to investigate the rotational anisotropic properties for lattice structures. The minimal regression coefficient can be treated as an indicator to evaluate anisotropy for lattice structures under rotation. This study demonstrates that the homogenized elastic model for lattice structures does not respond as an isotropic solid, and also does not have the elastic response under rotation of the widely-adopted orthotropic model on an element-by-element rotation basis. The homogenized elastic property under rotation can only be treated as an anisotropic model rather than an orthotropic model for TPMS-based lattice structures. Our results also show that urface-based TPMS lattice structures better follow an orthotropic model under rotation as compared with scaffold-based geometry due to the more sophisticated geometric configuration which may lead to uniform material distribution in the RVE.

Reference

[1] Krishnan, K., Lee, D. W., Al Teneji, M., & Al-Rub, R. K. A. (2022). Effective stiffness, strength, buckling and anisotropy of foams based on nine unique triple periodic minimal surfaces. *International Journal of Solids and Structures*, 238, 111418.

[2] Maskery, I., Aremu, A. O., Parry, L., Wildman, R. D., Tuck, C. J., & Ashcroft, I. A. (2018). Effective design and simulation of surface-based lattice structures featuring volume fraction and cell type grading. *Materials & Design*, 155, 220-232.

[3] Feng, J., Liu, B., Lin, Z., & Fu, J. (2021). Isotropic porous structure design methods based on triply periodic minimal surfaces. *Materials & Design*, 210, 110050.

[4] Abueidda, D. W., Al-Rub, R. K. A., Dalaq, A. S., Lee, D. W., Khan, K. A., & Jasiuk, I. (2016). Effective conductivities and elastic moduli of novel foams with triply periodic minimal surfaces. *Mechanics of Materials*, 95, 102-115.

[5] Chen, Z., Xie, Y. M., Wu, X., Wang, Z., Li, Q., & Zhou, S. (2019). On hybrid cellular materials based on triply periodic minimal surfaces with extreme mechanical properties. *Materials & design*, 183, 108109.

[6] Khaleghi, S., Dehnavi, F. N., Baghani, M., Safdari, M., Wang, K., & Baniassadi, M. (2021). On the directional elastic modulus of the TPMS structures and a novel hybridization method to control anisotropy. *Materials & Design*, 210, 110074.

[7] Wei, C., & Smith, D. E. (2023, October). Design of Spatially Varying Orientation Lattice Structures Using Triply Periodic Minimal. *In 2023 International Solid Freeform Fabrication Symposium.* https://utw10945. utweb. utexas. edu/2023-table-contents.

[8] Tran, K. Q., Le, T. D., Nguyen, N. V., & Nguyen-Xuan, H. (2024). Design of 3D rotating triply periodic minimal surface (RotTPMS) lattice plates: Meanings of crystalline rotations and porosity. *International Journal of Mechanical Sciences*, 109090.

[9] Ranganathan, Shivakumar I., and Martin Ostoja-Starzewski. "Universal elastic anisotropy index." *Physical review letters* 101.5 (2008): 055504.

[10] Wang, Yan. "Periodic surface modeling for computer aided nano design." *Computer-Aided Design* 39.3 (2007): 179-189.

[11] Moerman, Kevin M. "GIBBON: the geometry and image-based bioengineering add-on." *Journal of Open Source Software* 3.22 (2018): 506.

[12] The MathWorks Inc. (2022). MATLAB version: 9.13.0 (R2022b), Natick, Massachusetts: The MathWorks Inc. https://www.mathworks.com

[13] Dong, G., Tang, Y., & Zhao, Y. F. (2019). A 149 line homogenization code for three-dimensional cellular materials written in matlab. *Journal of Engineering Materials and Technology*, 141(1), 011005.

[14] Fisher, J. W., Miller, S. W., Bartolai, J., Simpson, T. W., & Yukish, M. A. (2023). Catalog of triply periodic minimal surfaces, equation-based lattice structures, and their homogenized property data. *Data in Brief*, 49, 109311.

[15] Tyrus, J. M., M. Gosz, and E. DeSantiago. "A local finite element implementation for imposing periodic boundary conditions on composite micromechanical models." *International Journal of Solids and Structures* 44.9 (2007): 2972-2989.

[16] Boise, C. M., D. A. Jack, and D. E. Smith. "A multiple anisotropic material finite element and its application to stiffness tensor predictions for woven composite lamina." *Composites Part A*: *Applied Science and Manufacturing*, 99 (2017): 208-220.

[17] Miehe, Christian, and Andreas Koch. "Computational micro-to-macro transitions of discretized microstructures undergoing small strains." *Archive of Applied Mechanics* 72 (2002): 300-317.

[19] Middleton, Joseph Ervin. Elastic property prediction of long fiber composites using a uniform mesh finite element method. University of Missouri-Columbia, 2008.

[20] Caselman, Elijah. Elastic property prediction of short fiber composites using a uniform mesh finite element method. Diss. University of Missouri--Columbia, 2007.

[21] Bond, Walter L. "The mathematics of the physical properties of crystals." *The Bell System Technical Journal* 22.1 (1943): 1-72.

[22] Walker, A. M., & Wookey, J. (2012). MSAT—A new toolkit for the analysis of elastic and seismic anisotropy. Computers & Geosciences, 49, 81-90.

[23] Roylance, D. (2001). Transformation of stresses and strains. Lecture notes for mechanics of materials.